Pressure- and temperature-driven phase transitions in HgTe quantum wells

S. S. Krishtopenko,[1,2] I. Yahniuk,[3] D. B. But,[2] V. I. Gavrilenko,[1,4] W. Knap,[2,3] and F. Teppe[2,*]

[1]*Institute for Physics of Microstructures, Russian Academy of Sciences, GSP-105, 603950 Nizhni Novgorod, Russia*

[2]*Laboratoire Charles Coulomb, UMR Centre National de la Recherche Scientifique 5221, University of Montpellier, 34095 Montpellier, France*

[3]*Institute of High Pressure Physics, Polish Academy of Sciences, Sokołowska 29/37 01-142 Warsaw, Poland*

[4]*Lobachevsky State University of Nizhni Novgorod, pr. Gagarina 23, 603950 Nizhni Novgorod, Russia*

(Received 15 July 2016; revised manuscript received 9 October 2016; published 1 December 2016)

We present theoretical investigations of pressure- and temperature-driven phase transitions in HgTe quantum wells grown on a CdTe buffer. Using the eight-band $\mathbf{k}\cdot\mathbf{p}$ Hamiltonian we calculate evolution of energy-band structure at different quantum well widths with hydrostatic pressure up to 20 kbars and temperature ranging up to 300 K. In particular, we show that, in addition to temperature, tuning of hydrostatic pressure allows us to drive transitions between semimetal, band insulator, and topological insulator phases. Our realistic band-structure calculations reveal that the band inversion under hydrostatic pressure and temperature may be accompanied by nonlocal overlapping between conduction and valence bands. The pressure and temperature phase diagrams are presented.

DOI: 10.1103/PhysRevB.94.245402

I. INTRODUCTION

Almost a decade ago a new class of materials, so-called topological insulators (TIs), was predicted [1,2]. TIs possess a band gap for the bulk states and gapless edge states. These edge states are protected against single-particle perturbations by time-reversal symmetry [1–6]. TI systems can be found in materials, in which the conduction and valence bands have opposite parity and a change in the band ordering occurs [4].

The first TIs discovered were based on HgTe/Cd(Hg)Te quantum wells (QWs) [4,5]. This two-dimensional (2D) system can be tuned from the trivial band insulator (BI) to the 2D TI phase by changing the QW width d. The origin of the 2D TI phase is caused by the inverted band structure of HgTe, which leads to a peculiar size quantization in HgTe/Cd(Hg)Te QWs. Specifically, as d is varied, the lowest 2D sub-band, formed by coupling of conduction-band (Γ_6) states with light-hole (Γ_8) states and defined as an electronlike level (E1 sub-band), crosses the top sub-band of heavy-hole (Γ_8) states (H1 sub-band) [4]. When d exceeds the critical width d_c the E1 sub-band falls below the H1 sub-band and the 2D system has inverted band structure [see Fig. 1(c)]. The critical width also depends on the crystallographic orientation and buffer material, on which the QW is grown. For $HgTe/Cd_{0.7}Hg_{0.3}$ QWs grown on a CdTe buffer, $d_c \approx 6.5$ and 6.3 nm for (001) and (013) orientations, respectively. In narrow HgTe QWs ($d < d_c$), a conventional alignment of electronic states (CdTe-like) with BI phase can be obtained [see Fig. 1(a)]. Thus, a topological phase transition occurs at the critical thickness d_c, at which the band gap is absent and the system is characterized by the linear dispersion of massless Dirac fermions [7].

In wide HgTe/Cd(Hg)Te QWs the side maximum of the valence band overlaps with the conduction band [see Fig. 1(e)], while $d = d_{SM}$ corresponds to the indirect gapless state [Fig. 1(d)]. A semimetal (SM) phase at $d > d_{SM}$ is then formed when the Fermi level crosses both the valence and conduction bands [8–10]. Recent finding proves [8,9] that the SM phase is a universal property of wide HgTe QWs independent of the surface orientation. Additionally, the overlapping of the valence and conduction bands, thus the SM phase, is very sensitive to the strain effects [9] caused by the lattice mismatch of HgTe and CdTe.

A reliable fingerprint of the band inversion is the characteristic behavior of a particular pair of Landau levels (LLs), so-called zero-mode LLs [5,7], under applied magnetic field B. Below a critical field value B_c, the lowest zero-mode LL has electronlike character and arises from the valence band, while the highest zero-mode LL has a heavy-hole-like character and splits from the conduction band. In these inverted band conditions, the topological edge states are still present, although they are no longer protected by time-reversal symmetry [11–13]. With increasing magnetic field, the zero-mode LLs cross each other at $B = B_c$. Above this magnetic field value the band structure becomes normal and only the trivial quantum Hall insulator can be found.

The changing of external parameters may offer an effective way for fine tuning of phase transition between BI, TI, and SM phases keeping intrinsic parameters of the QW. The latter can be highly desirable for future topological devices [14]. It has been recently demonstrated that a transition between BI and TI phases can be either driven by electric field [15,16], applied along the growth direction, or driven by temperature [17,18]. However, the mentioned works were focused on the evolution of the band structure due to transition between BI and TI phases only, while temperature and electric field effects in the SM phase were ignored.

In this work, we are not only focused on temperature effects on the *nonlocal* band structure but also propose to use hydrostatic pressure for fine tuning of the transitions between BI, TI, and SM phases. We discover that at reasonable values of hydrostatic pressure and temperature, the band inversion at the Γ point of the Brillouin zone does not lead to the formation of the TI phase in HgTe QWs. We also show the evolution of

*frederic.teppe@umontpellier.fr

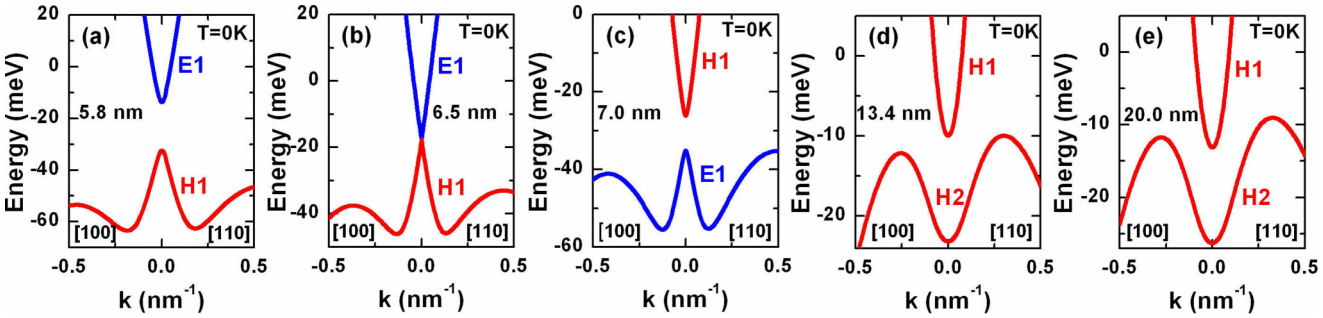

FIG. 1. Typical band structure of (001)-oriented HgTe QWs at zero temperature and at different QW width: (a) BI phase, $d < d_c$, (b) Dirac cone, $d = d_c$, (c) TI phase $d > d_c$, (d) gapless state, $d = d_{\rm SM}$, and (d) SM phase, $d > d_{\rm SM}$. The electronlike E1 sub-band is shown in blue, while red curves correspond to the heavy-hole sub-bands. In the panels (d) and (e), the E1 sub-band lies significantly lower in energy. Here, we do not differ the TI state, in which the band gap is defined by the gap between H1 and E1 sub-bands, and TI states, in which the E1 sub-band lies below several heavy-hole-like sub-bands [19].

the critical magnetic field B_c with pressure and temperature in HgTe QWs of different width.

II. THEORETICAL BASIS

To describe the sub-band nonparabolicity [7,8,10,20] and the spin-orbit interaction effects in HgTe QWs, we use the eight-band $\mathbf{k}\cdot\mathbf{p}$ Hamiltonian for the envelope wave functions, which takes into account the interaction between Γ_6, Γ_8, and Γ_7 bands. Further, we consider QWs grown on the $[0lk]$ plane (l and k are integer numbers), which includes the most prevalent cases of (001)- [5–7,18,20] and (013)-oriented [8,10,21,22] structures. We note that the previously reported six-band $\mathbf{k}\cdot\mathbf{p}$ Hamiltonian [23,24] for general $(0lk)$ orientation considers only Γ_6 and Γ_8 bands and includes interaction with the Γ_7 band only via the second-order perturbation theory.

Although electronic states in HgTe QWs can be indeed qualitatively described by the six-band $\mathbf{k}\cdot\mathbf{p}$ Hamiltonian, to calculate quantitative values of hydrostatic pressure and temperature, corresponding to the transition between BI, TI, and SM phases, we also include the Γ_7 band in the Hamiltonian. The latter has significant effect on the electronlike states in HgTe QWs [25], while for the band structure of the bulk HgCdTe-based materials, effect of the Γ_7 band can be neglected [26].

The matrix elements of the eight-band $\mathbf{k}\cdot\mathbf{p}$ Hamiltonian depend on momentum operators k_x, k_y, and k_z; conduction- and valence-band edges $E_c(z)$ and $E_v(z)$; spin-orbit energy $\Delta(z)$; Kane energy E_P; and the modified Luttinger parameters γ_1, γ_2, γ_3, κ, and F. We also take into account effects of strain, resulting from mismatch of the lattice parameters in the given layer of heterostructure a_L and the buffer a_0. The strain terms in the Hamiltonian include the hydrostatic a_c and a_v and uniaxial b and d deformation potentials, as well as the strain tensor with components ϵ_{ij}. In the work, we focus on $HgTe/Cd_{0.7}Hg_{0.3}Te$ QWs grown on a CdTe buffer. The explicit form of the eight-band $\mathbf{k}\cdot\mathbf{p}$ Hamiltonian is given in Ref. [25]. We should point out that we have neglected in our Hamiltonian the linear-in-$\mathbf{k}$ terms, resulting from the bulk inversion asymmetry (BIA) in bulk zinc-blende crystals [27]. In the models with BIA [22], the crossing between zero-mode LLs at B_c is avoided. The latter gives rise to specific behavior of magneto-optical transitions from the zero-mode LLs in the vicinity of critical magnetic field [10,22,28]. If magnetic field either exceeds B_c or remains significantly lower than the critical field, effects of BIA are negligible. Further, effects of BIA are therefore ignored.

To perform band-structure calculations of HgTe/Cd(Hg)Te QWs at different values of hydrostatic pressure P and temperature T, we take into account the dependencies of all relevant band parameters and the changes in the valence-band offset (VBO) Ω between HgTe and CdTe. The VBO defines the misalignment of energy-band gaps in adjacent layers of the QW. By setting the energy of Γ_8 band at $k = 0$ in unstrained bulk HgTe to zero, Ω equals to the valence-band edge $E_v(z)$ in the given layer. According to Latussek *et al.* [29] and Becker *et al.* [30] Ω has a linear dependence on P and T:

$$\Omega(P,T) = \Omega_0 + \beta_P P + \beta_T T, \tag{1}$$

where Ω_0 is the VBO at $T = 0$ and $P = 0$ (counted from atmospheric pressure), while β_P and β_T are independent of pressure and temperature. It is worth noting that β_P is known only for VBO between HgTe and $Cd_{0.7}Hg_{0.3}Te$ [29]. Thus, by assuming β_P to vary linearly with x for $Cd_xHg_{1-x}Te$ alloy, we extract the value for VBO between HgTe and CdTe.

Normally the pressure dependence of the band gap $E_g = E_c - E_v$ in bulk materials is analyzed by means of a quadratic equation:

$$E_g(P,T) = E_g^{(0)}(T) + \alpha_0 P + \alpha_1 P^2, \tag{2}$$

in which α_0 and α_1 depend on the range of pressures over which the analysis is conducted [29]. Previously, α_0 and α_1 for bulk HgTe have been determined from pressure dependence of inter-sub-band transitions in $HgTe/Cd_{0.7}Hg_{0.3}Te$ superlattices at $P < 2.5$ GPa [29]. By analyzing experimental results, α_0 and α_1 were obtained to be equal to 87.2 meV/GPa and -4.61 meV/GPa^2, respectively. For bulk CdTe, in accordance with Eqs. (7) and (8) in Ref. [29], we set α_0 and α_1 to 81.0 meV/GPa and -4.96 meV/GPa^2, respectively. The temperature dependence of $E_g^{(0)}(T)$ on x for $Cd_xHg_{1-x}Te$ alloy is determined from the empirical expression according to Laurenti *et al.* [35].

Previous studies have shown pronounced dependence of overlapping between valence and conduction bands on lattice-mismatch deformation in the SM phase in wide HgTe QWs [9]. Therefore, to describe the temperature and pressure effects on electronic states in the SM phase, one should accurately take

TABLE I. Band parameters for HgTe and CdTe independent of hydrostatic pressure and temperature.

Parameters	CdTe	HgTe	Parameters	CdTe	HgTe
α_0 (meV/GPa)	81[a]	87.2[a]	α_1 (meV/GPa^2)	−4.96[a]	−4.61[a]
β_T (meV/K)	0.4[b]	0	β_P (meV/GPa)	35.7[c]	0
Ω_0 (eV)	−0.57	0	a_{300K} (Å)	6.4823[d]	6.4615[d]
Δ (eV)	0.91	1.08	F	0	−0.09
E_P (eV)	18.8[e]	18.8[e]	κ	−1.31	−0.4
dc_{11}/dP	4.44[f]	3.30[g]	γ_1	1.47	4.1
dc_{12}/dP	2.62[f]	4.10[g]	γ_2	−0.28	0.5
dc_{44}/dP	1.92[f]	−0.12[g]	γ_3	0.03	1.3
a_c (eV)	−2.925	−2.380	a_v (eV)	0	1.31
b (eV)	−1.2	−1.5	d (eV)	−5.4	−2.5

[a]Ref. [29].
[b]Ref. [30].
[c]Calculated by using results of Ref. [29].
[d]Ref. [31].
[e]Recent results [32] show temperature independence of E_P in HgCdTe alloys.
[f]Calculated by using results of Ref. [33].
[g]Ref. [34].

into account the dependence of elastic constants and lattice parameters on P and T. In this paper, the elastic constants c_{ij} are assumed to have linear dependence on P [33,34]:

$$c_{ij}(P,T) = c_{ij}^{(0)}(T) + P\frac{dc_{ij}}{dP}, \tag{3}$$

while the temperature dependencies of $c_{ij}^{(0)}(T)$ describe experimental data [31]. Here, dc_{ij}/dP are assumed to be independent on P and T. The linear dependence on P in Eq. (3) allows us to use Murnaghan's equation of state for changing in the lattice parameter a_L in the given layer with hydrostatic pressure:

$$a_L(P,T) = a_L^{(0)}(T)\left[1 + P\frac{B_0'}{B_0(T)}\right]^{-1/3B_0'}, \tag{4}$$

where $B_0(T) = (c_{11}(T) + 2c_{12}(T))/3$ is the bulk modulus and $B_0' = (dc_{11}/dP + 2dc_{12}/dP)/3$.

Temperature dependence of $a_L^{(0)}(T)$ is obtained by solving the differential equation

$$\alpha(T) = \frac{1}{a_L^{(0)}(T)}\frac{da_L^{(0)}(T)}{dT} \tag{5}$$

with condition

$$a_L^{(0)}(300K) = a_{300K}.$$

Here $\alpha(T)$ is the thermal expansion coefficient, taken from experimental data [31]. Other band-structure parameters for HgTe and CdTe, which are supposed to be independent on T and P, are listed in Table I. As in Ref. [20], the band parameters are assumed to be a piecewise function along the growth direction and to vary linearly with x in $Cd_xHg_{1-x}Te$ alloy.

III. RESULTS AND DISCUSSIONS

A. Topological insulator phase

Inversion of electronic sub-bands at the Γ point and nonzero band gap are essential for a formation of TI phase in HgTe QWs [4,5]. Therefore, we first focus on the effect of changing of the sub-band ordering with hydrostatic pressure and temperature. The top panels in Fig. 2 present energies of the electronlike E1; the heavy-hole-like H1, H2, H3; and the light-hole-like LH1 sub-bands at the Γ point as a function of P and T, calculated for 8-nm $HgTe/Cd_{0.7}Hg_{0.3}Te$ QWs. This figure shows the similarity of pressure and temperature effects on the band ordering.

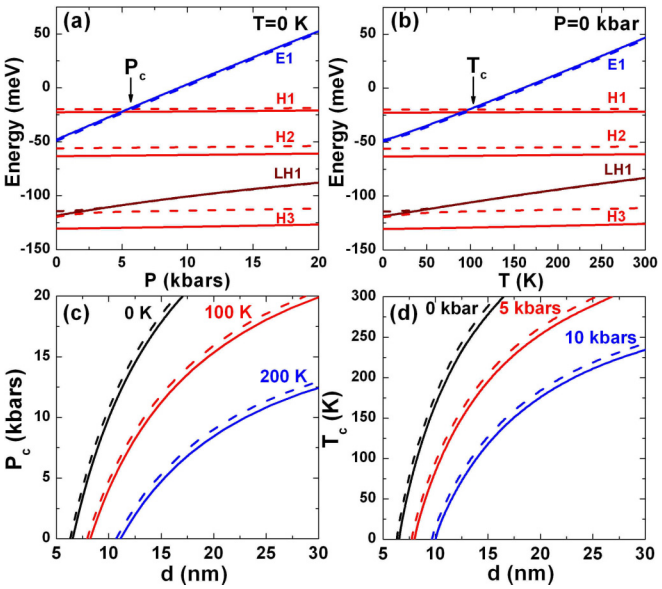

FIG. 2. (a,b) Band edge of the electron-like E1; the heavy-hole-like H1, H2, and H3; and the light-hole-like LH1 sub-bands at the Γ point in 8-nm $HgTe/Cd_{0.7}Hg_{0.3}Te$ QWs as a function of hydrostatic pressure (a) and temperature (b). (c,d) Dependence of critical pressure P_c and temperature T_c, at which the Dirac cone in the Γ point arises [see Fig. 1(b)], as a function of d for $HgTe/Cd_{0.7}Hg_{0.3}Te$ QWs. In all the panels, solid curves represent the calculations for (001)-oriented QWs, while the dashed curves correspond to the structures grown on the [013] plane.

At small values of P and T, the band structure remains inverted and TI phase in HgTe QW survives. However, strong pressure and temperature dependence of the E1 sub-band results in the crossing between E1 and H1 sub-bands at some critical values of pressure P_c and temperature T_c. In this case, energy dispersion in the vicinity of the Γ point is linear in quasimomentum [see Fig. 1(b)], and further increasing of P and T puts the HgTe QW into BI phase with direct band ordering. The difference in P_c and T_c for (001)- and (013)-oriented QWs is mostly related with lattice-mismatch strain, which also depends on the growth direction [see Eq. (3) in Ref. [25]]. Two bottom panels in Fig. 2 demonstrate that both P_c and T_c have a strong nonlinear dependence on the QW width. Moreover, P_c and T_c depend on temperature and pressure, respectively; both quantities significantly decrease with T and P at given QW width.

As mentioned above, the band inversion at the Γ point leads to the crossing of zero-mode LLs in critical magnetic field B_c [5,7]. If the $B > B_c$, HgTe QW has a direct band ordering, while below B_c the band structure remains inverted and the helical edge state still exists [11–13]. The top panel in Fig. 3 shows LLs in the (001) $HgTe/Cd_{0.7}Hg_{0.3}Te$ QW calculated for zero P and T values. The numbers over the curves correspond to the LL indices [25]. Two red curves are the zero-mode LLs, which are identified within a simplified approach, based on the 2D Dirac-type Hamiltonian [4]. The panel below displays B_c as a function of QW width d for the (001)- and (013)-oriented QWs for zero pressure and temperature.

The bottom panels in Fig. 3 show the dependence of B_c on P and T for the 8- and 12-nm QWs of different orientations. It is seen that critical magnetic field decreases with pressure and temperature. The latter is related with the collapse of the gap between E1 and H1 sub-bands, if pressure and temperature tend to P_c and T_c, respectively (see Fig. 2). Above P_c and T_c, the band structure is direct and the zero-mode LLs are not crossed [7].

So far, we have considered ordering of electronic sub-bands in HgTe QWs in the vicinity of $k = 0$, driven by hydrostatic pressure and temperature. However, such *local* picture does not account for all the electronic properties of HgTe QWs in the TI phase. For instance, if the width d increases, the QW has indirect band gap due to arising of the side maxima in the valence band, whose positions depend on the growth direction [36].

To illustrate the differences, arising in valence bands for (001)- and (013)-oriented HgTe QWs, we provide a three-dimensional plot of the band structure and contour lines for the 8-nm QWs at $P = 0$ and $T = 0$ (see Fig. 4). For both QWs, the conduction band has an isotropic energy-momentum law. The valence band is anisotropic with four side maxima shifted from the Γ point. However, the valence band in the (013)-oriented QW is highly anisotropic even at small values of quasimomentum. Due to low-symmetry growth orientation, positions of the four side maxima in (013)-oriented QWs depend also on the QW width. Thus, to calculate the values of the indirect band gap in the (013)-oriented QW, one should first find the crystallographic direction, corresponding to the side maxima at given QW width.

On the other hand, positions of the maxima in the (001) QWs are independent of the QW width. They always lie

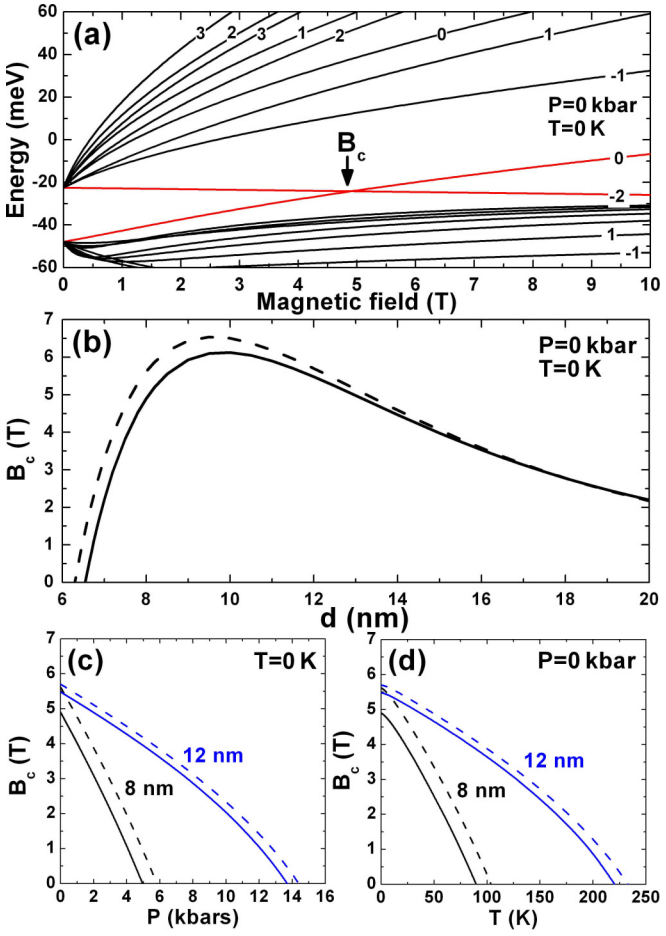

FIG. 3. (a) Landau levels for (001)-oriented $HgTe/Cd_{0.7}Hg_{0.3}Te$ QWs of 8-nm thickness at $T = 0$ K and $P = 0$ kbar. A pair of zero-mode LLs is shown by red curves. (b) A critical field B_c as a function of QW width d at zero pressure and temperature. (c,d) A critical field B_c as a function of hydrostatic pressure and temperature for 8- and 12-nm QWs. The solid curves in the panels (b–d) display the calculations for (001)-oriented QWs, while the dashed curves correspond to the (013)-oriented structures.

along (110), $(\bar{1}10)$, $(1\bar{1}0)$, and $(\bar{1}\bar{1}0)$ directions, which are all equivalent. The latter is caused by the fact that anisotropic terms in the eight-band $\mathbf{k} \cdot \mathbf{p}$ Hamiltonian for (001)-oriented structures are independent of k_z [20]. Because of the easier calculations, we consider the pressure and temperature effects on the *nonlocal* band structure only for (001)-oriented HgTe QWs. Such effects for (013)-oriented QWs are expected to be qualitatively the same. We want to stress that all the disparities between different orientations are related with the valence band. They concern two main characteristics: (i) positions of the side maxima in the valence band and (ii) anisotropy of energy dispersion in the valence sub-band at small quasimomentum. However, detailed quantitative calculations for such low-symmetry orientation are very time consuming.

Figure 5 shows indirect band gap in HgTe QWs of different widths as a function of hydrostatic pressure and temperature. It is clear that the band-gap evolution strongly depends on the QW width. For the QWs with direct band gap, the band gap increases with P and T: from the negative values if the

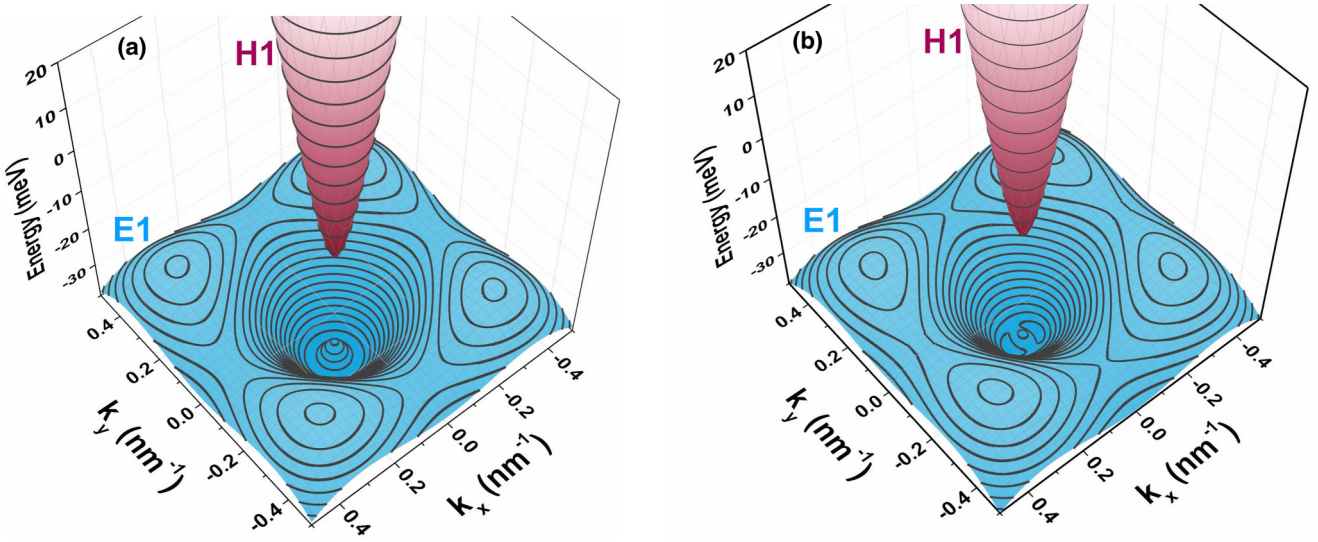

FIG. 4. Band structure and contour lines for HgTe/$Cd_{0.7}Hg_{0.3}$Te QWs of 8-nm width, grown on (a) [001] and (b) [013] planes for $T = 0$ and $P = 0$. The E1 sub-band is shown in blue, and the red surface corresponds to the H1 sub-band. The x and y axes for the (001) QW are oriented along (100) and (010) crystallographic directions, while for the (013) QW, the axes correspond to the directions of (100) and (03$\bar{1}$), respectively.

band structure is inverted, and from the positive values in the case of the band insulator phase. If HgTe QW is wide enough, the system has an indirect band gap, which has a weaker dependence on P and T than the gap at the Γ point (see the 8-nm-thick QW). At specific values of pressure and temperature, the side maxima in the valence band are placed below the top at $k = 0$. Further increasing of P or T results in rising of the band gap almost linearly with pressure and temperature.

The indirect gap in the 12-nm HgTe QW equals to zero in a wide range of pressure and temperature. This holds as long as the gap at the Γ point does not vanish (see the dashed curves in Fig. 5). Further increasing of P and T puts the system into the BI phase with a sublinear dependence of the band gap on hydrostatic pressure and temperature. We note that the gap at the Γ point also features a nonmonotonic behavior, which is related to swapping of E1 and H2 sub-bands. The indirect band gap is very sensitive to the strain effects resulted from difference in lattice constants in the QW, barriers, and buffer.

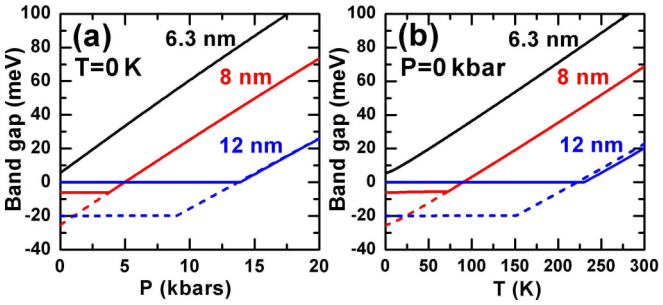

FIG. 5. The band gap in HgTe/$Cd_{0.7}Hg_{0.3}$Te QWs grown on a (001) CdTe buffer as a function of (a) P and (b) T, calculated for different QW widths. The negative band-gap values correspond to inverted band structure. The dashed curve shows the evolution of the gap at the Γ point.

For instance, a 12-nm HgTe/$Cd_{0.7}Hg_{0.3}$Te QW grown on a CdTe buffer has zero indirect band gap at small values of P and T (see Fig. 5), while for the QW grown on another buffer, the band gap may be opened [18].

B. Semimetal phase

In wide HgTe QWs the indirect band gap vanishes and the system is characterized by nonlocal overlapping between conduction and valence bands. As mentioned above, the latter case is called the SM phase [8,9]. Typically, it arises when the E1 level lies below several heavy-hole-like sub-bands. Let us now focus on the pressure and temperature evolution of the overlapping between conduction and valence bands in the SM phase.

For this purpose, we consider a 20-nm HgTe QW, in which existence of the SM phase at low temperatures was demonstrated in a number of experiments [8,9,37–39]. Figure 6 represents the calculations of nonlocal overlapping between conduction and valence sub-bands as a function of P and T. In contrast to the band-gap evolution, pressure and temperature have different effects on the band overlapping. Increasing of the pressure reduces the overlapping at $T = 0$, while the temperature increases the overlapping values for zero hydrostatic pressure. Variation of both P and T may modify the evolution of overlapping significantly. The latter is demonstrated by the red and blue curves in Fig. 6. It is seen that at specific values of P and T, the band overlapping decreases dramatically.

The origin of such decrease is related with a change of the band structure from inverted into the normal one under joint effect of pressure and temperature. Two bottom panels in Fig. 6 show pressure and temperature evolution of the overlapping and the band gap at the Γ point at $T = 200$ K and $P = 10$ kbars, respectively. One can see that, at the values of P and T, corresponding to the decreasing of the band

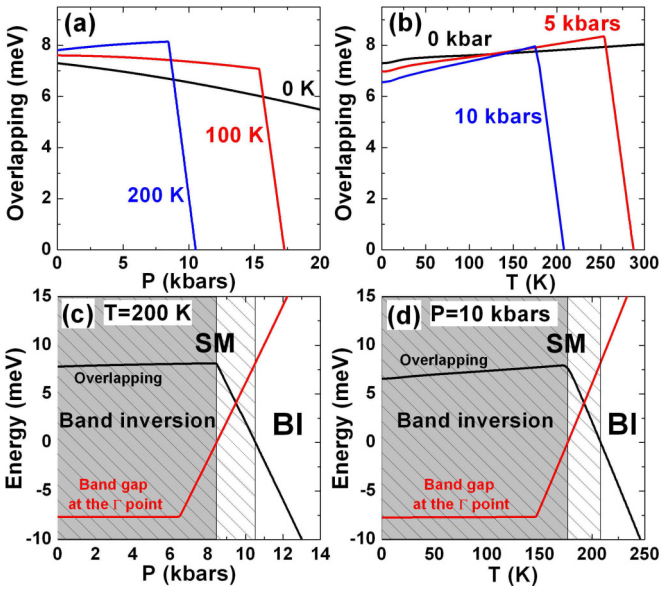

FIG. 6. (a,b) Overlapping between conduction and valence sub-bands in 20-nm $HgTe/Cd_{0.7}Hg_{0.3}Te$ QWs, grown on a (001) CdTe buffer as a function of (a) hydrostatic pressure and (b) temperature. (c,d) Overlapping (black curves) and band gap at the Γ point (red curves): (c) as a function of P for $T = 200$ K and (d) as a function of T for $P = 10$ kbars. The negative overlapping values in the panels (c,d) define the indirect band gap. The white-open regions are connected with the BI phase, the striped regions correspond to the SM phase, while the gray regions define the range of P and T with the inverted band structure.

overlapping, the band-gap energy at the Γ point changes sign. We note that the normal band ordering is defined by positive band gap at the Γ point even if the indirect band gap equals to zero. Thus, the white-striped regions in Figs. 6(c) and 6(d), characterized by both positive values of the overlapping and the gap at $k = 0$, correspond to the SM phase but with *normal* band ordering.

The SM phase with direct band ordering, arising under hydrostatic pressure and temperature, has not been predicted before. Evolution of the band structure of the 20-nm HgTe QW due to pressure-driven phase transition into this specific phase at $T = 200$ K is shown in Fig. 7. It is seen that the

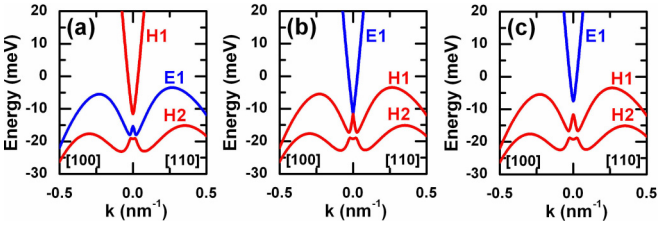

FIG. 7. Evolution of the band structure in 20-nm $HgTe/Cd_{0.7}Hg_{0.3}Te$ QWs, grown on a (001) CdTe buffer, at $T = 200$ K with hydrostatic pressure: (a) $P = 7.5$ kbars (the SM phase with inverted band structure); (b) $P = 8.45$ kbars (the SM phase with the Dirac cone in the Γ point); and (c) $P = 9.5$ kbars (the SM phase with direct band ordering). Electron-like and heavy-hole-like sub-bands are shown in blue and red, respectively.

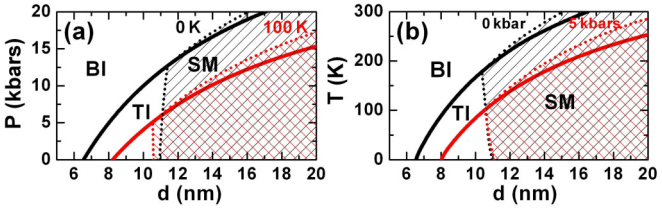

FIG. 8. (a) Pressure and (b) temperature phase diagram for (001) $HgTe/Cd_{0.7}Hg_{0.3}Te$ QWs, grown on a CdTe buffer. The solid curves correspond to the arising of the Dirac cone at the Γ point. The dotted curves conform to a formation of the gapless states, shown in Fig. 1(d).

band inversion at the Γ point is accompanied by nonlocal overlapping of the conduction and valence bands. We note that such phase transition cannot be described within the simplified 2D Dirac-type model [4], because it considers the bulk and edge states only in the vicinity of $k = 0$. Moreover, any known simplified 2D models [4,6,23,40] are not generally applicable to this case. Therefore, even the qualitative picture of the edge states in the SM phase is unknown.

Figure 8 presents pressure and temperature phase diagrams for (001) $HgTe/Cd_{0.7}Hg_{0.3}Te$ QWs grown on a CdTe buffer. The white-open regions in all the panels correspond to the insulator phases, while the striped regions are the SM phase with the overlapping of conduction and valence bands. First, it is seen that in a wide range of QW width d, tuning of hydrostatic pressure and temperature allows one to drive transitions between SM, BI, and TI phases. The second point is that the TI phase in HgTe QWs exists only in the finite ranges of P and T. Indeed, at given value of hydrostatic pressure, there is a limit temperature above which the TI phase collapses due to nonlocal overlapping between the conduction and valence bands. Our calculations, performed for $HgTe/Cd_xHg_{1-x}Te$ QWs at different values of Cd concentration x, show that such limit temperature value does not exceed room temperature. The diagrams in Fig. 8 evidence that variation of d at high pressure and temperature drives the system from BI into SM, avoiding a TI phase.

IV. CONCLUSIONS

With accurate calculations on the basis of the eight-band $\mathbf{k} \cdot \mathbf{p}$ Hamiltonian, we have theoretically studied effect of hydrostatic pressure and temperature on the band structure and Landau levels in HgTe QWs, grown along (001) and (013) crystallographic orientations. We have demonstrated that variation of these two external parameters can be efficiently used for driving transitions between semimetal, band insulator, and topological insulator phases. We have shown the existence of a topological insulator phase only in the finite range of P and T. At high pressure and temperature, variation of HgTe QW width drives the system from band insulator into the semimetal, avoiding the topological insulator phase.

At specific values of pressure and temperature, our band-structure calculations reveal that the band inversion in HgTe QWs does not lead to formation of the topological insulator phase due to accompanying nonlocal overlapping between conduction and valence bands. The pressure and temperature diagrams for (001) $HgTe/Cd_{0.7}Hg_{0.3}Te$ QWs grown on a CdTe

buffer have been presented. Our results provide a theoretical basis for future magnetotransport and magnetospectroscopy experimental works [41–43].

ACKNOWLEDGMENTS

This work was supported by the CNRS through Laboratoire International Associé (LIA) "TERAMIR" and the postdoctoral prolongation program of the Institute of Physics, the Languedoc-Roussillon region via the Gepeto Terahertz platform, the Russian Academy of Sciences, the nonprofit Dynasty foundation, the Russian Foundation for Basic Research (Grants No. 15-02-08274, No. 15-52-16012, and No. 16-02-00672), the Russian Scientific Foundation (Grant No. 16-12-10317), Russian Ministry of Education and Science (Grants No. MK-6830.2015.2 and No. HIII-1214.2014.2), and the HARMONIA project of National Science Center (Poland), allocated on the basis of Decision No. DEC-2013/10/M/ST3/00705.

[1] C. L. Kane and E. J. Mele, Phys. Rev. Lett. **95**, 146802 (2005).
[2] C. L. Kane and E. J. Mele, Phys. Rev. Lett. **95**, 226801 (2005).
[3] B. A. Bernevig and S.-C. Zhang, Phys. Rev. Lett. **96**, 106802 (2006).
[4] B. A. Bernevig, T. L. Hughes, and S.-C. Zhang, Science **314**, 1757 (2006).
[5] M. König, S. Wiedmann, C. Brüne, A. Roth, H. Buhmann, L. W. Molenkamp, X.-L. Qi, and S.-C. Zhang, Science **318**, 766 (2007).
[6] M. König, H. Buhmann, L. W. Molenkamp, T. Hughes, C.-X. Liu, X.-L. Qi, and S.-C. Zhang, J. Phys. Soc. Jpn. **77**, 031007 (2008).
[7] B. Büttner, C. Liu, G. Tkachov, E. Novik, C. Brüne, H. Buhmann, E. Hankiewicz, P. Recher, B. Trauzettel, S. Zhang, and L. Molenkamp, Nat. Phys. **7**, 418 (2011).
[8] Z. Kvon, E. Olshanetsky, D. Kozlov, N. Mikhailov, and S. Dvoretskii, JETP Lett. **87**, 502 (2008).
[9] Z. D. Kvon, E. B. Olshanetsky, E. G. Novik, D. A. Kozlov, N. N. Mikhailov, I. O. Parm, and S. A. Dvoretsky, Phys. Rev. B **83**, 193304 (2011).
[10] M. Zholudev, F. Teppe, M. Orlita, C. Consejo, J. Torres, N. Dyakonova, M. Czapkiewicz, J. Wróbel, G. Grabecki, N. Mikhailov, S. Dvoretskii, A. Ikonnikov, K. Spirin, V. Aleshkin, V. Gavrilenko, and W. Knap, Phys. Rev. B **86**, 205420 (2012).
[11] G. Tkachov and E. M. Hankiewicz, Phys. Rev. Lett. **104**, 166803 (2010).
[12] J.-c. Chen, J. Wang, and Q.-f. Sun, Phys. Rev. B **85**, 125401 (2012).
[13] B. Scharf, A. Matos-Abiague, and J. Fabian, Phys. Rev. B **86**, 075418 (2012).
[14] L. A. Wray, Nat. Phys. **8**, 705 (2012).
[15] W. Yang, K. Chang, and S.-C. Zhang, Phys. Rev. Lett. **100**, 056602 (2008).
[16] J. Li and K. Chang, Appl. Phys. Lett. **95**, 222110 (2009).
[17] P. Sengupta, T. Kubis, Y. Tan, M. Povolotskyi, and G. Klimeck, J. Appl. Phys. **114**, 043702 (2013).
[18] S. Wiedmann, A. Jost, C. Thienel, C. Brüne, P. Leubner, H. Buhmann, L. W. Molenkamp, J. C. Maan, and U. Zeitler, Phys. Rev. B **91**, 205311 (2015).
[19] E. B. Olshanetsky, Z. D. Kvon, G. M. Gusev, A. D. Levin, O. E. Raichev, N. N. Mikhailov, and S. A. Dvoretsky, Phys. Rev. Lett. **114**, 126802 (2015).
[20] E. G. Novik, A. Pfeuffer-Jeschke, T. Jungwirth, V. Latussek, C. R. Becker, G. Landwehr, H. Buhmann, and L. W. Molenkamp, Phys. Rev. B **72**, 035321 (2005).
[21] A. M. Kadykov, F. Teppe, C. Consejo, L. Viti, M. S. Vitiello, S. S. Krishtopenko, S. Ruffenach, S. V. Morozov, M. Marcinkiewicz, W. Desrat, N. Dyakonova, W. Knap, V. I. Gavrilenko, N. N. Mikhailov, and S. A. Dvoretsky, Appl. Phys. Lett. **107**, 152101 (2015).
[22] M. S. Zholudev, F. Teppe, S. V. Morozov, M. Orlita, C. Consejo, S. Ruffenach, W. Knap, V. I. Gavrilenko, S. A. Dvoretskii, and N. N. Mikhailov, JETP Lett. **100**, 790 (2015).
[23] O. E. Raichev, Phys. Rev. B **85**, 045310 (2012).
[24] K.-M. Dantscher, D. A. Kozlov, P. Olbrich, C. Zoth, P. Faltermeier, M. Lindner, G. V. Budkin, S. A. Tarasenko, V. V. Bel'kov, Z. D. Kvon, N. N. Mikhailov, S. A. Dvoretsky, D. Weiss, B. Jenichen, and S. D. Ganichev, Phys. Rev. B **92**, 165314 (2015).
[25] See Supplemental Material at http://link.aps.org/supplemental/10.1103/PhysRevB.94.245402 for the general form of the eight-band $\mathbf{k}\cdot\mathbf{p}$ Hamiltonian and details of band-structure and Landau-level calculations.
[26] J. D. Malcolm and E. J. Nicol, Phys. Rev. B **92**, 035118 (2015).
[27] M. H. Weiler, *Defects, (HgCd)Se, (HgCd)Te*, edited by R. K. Willardson and A. C. Beer, Semiconductors and Semimetals Vol. 16 (Academic, New York, 1981), p. 119.
[28] M. Orlita, K. Masztalerz, C. Faugeras, M. Potemski, E. G. Novik, C. Brüne, H. Buhmann, and L. W. Molenkamp, Phys. Rev. B **83**, 115307 (2011).
[29] V. Latussek, C. R. Becker, G. Landwehr, R. Bini, and L. Ulivi, Phys. Rev. B **71**, 125305 (2005).
[30] C. R. Becker, V. Latussek, A. Pfeuffer-Jeschke, G. Landwehr, and L. W. Molenkamp, Phys. Rev. B **62**, 10353 (2000).
[31] *Mercury Cadmium Telluride—Growth, Properties and Applications*, edited by Peter Capper and James Garland (Wiley, New York, 2011).
[32] F. Teppe, M. Marcinkiewicz, S. S. Krishtopenko, S. Ruffenach, C. Consejo, A. M. Kadykov, W. Desrat, D. But, W. Knap, J. Ludwig, S. Moon, D. Smirnov, M. Orlita, Z. Jiang, S. V. Morozov, V. I. Gavrilenko, N. N. Mikhailov, and S. A. Dvoretskii, Nat. Commun. **7**, 12576 (2016).
[33] E. Deligoz, K. Colakoglu, and Y. Ciftci, Physica B **373**, 124 (2006).
[34] S. Adachi, *Properties of Group-IV, III-V and II-VI Semiconductors*, edited by Peter Capper, Safa Kasap, and Arthur Willoughby (Wiley, New York, 2005).
[35] J. P. Laurenti, J. Camassel, A. Bouhemadou, B. Toulouse, R. Legros, and A. Lusson, J. Appl. Phys. **67**, 6454 (1990).
[36] A. Pfeuffer-Jeschke, Ph.D. thesis, University of Wurzburg, 2000.

[37] G. M. Minkov, A. V. Germanenko, O. E. Rut, A. A. Sherstobitov, S. A. Dvoretski, and N. N. Mikhailov, Phys. Rev. B **88**, 155306 (2013).

[38] E. B. Olshanetsky, Z. D. Kvon, Y. A. Gerasimenko, V. A. Prudkoglyad, V. M. Pudalov, N. N. Mikhailov, and S. A. Dvoretsky, JETP Lett. **98**, 843 (2014).

[39] A. Kononov, S. V. Egorov, Z. D. Kvon, N. N. Mikhailov, S. A. Dvoretsky, and E. V. Deviatov, Phys. Rev. B **93**, 041303 (2016).

[40] S. A. Tarasenko, M. V. Durnev, M. O. Nestoklon, E. L. Ivchenko, J.-W. Luo, and A. Zunger, Phys. Rev. B **91**, 081302 (2015).

[41] A. V. Ikonnikov, S. S. Krishtopenko, O. Drachenko, M. Goiran, M. S. Zholudev, V. V. Platonov, Y. B. Kudasov, A. S. Korshunov, D. A. Maslov, I. V. Makarov, O. M. Surdin, A. V. Philippov, M. Marcinkiewicz, S. Ruffenach, F. Teppe, W. Knap, N. N. Mikhailov, S. A. Dvoretsky, and V. I. Gavrilenko, Phys. Rev. B **94**, 155421 (2016).

[42] M. Marcinkiewicz, S. Ruffenach, S. S. Krishtopenko, A. M. Kadykov, C. Consejo, J. Torres, D. But, N. Dyakonova, D. Coquillat, W. Knap, A. V. Ikonnikov, K. E. Spirin, S. V. Morozov, V. I. Gavrilenko, N. N. Mikhailov, S. A. Dvoretsky, and F. Teppe (unpublished).

[43] I. Yahniuk, S. S. Krishtopenko, G. Grabecki, M. Majewicz, J. Wrobel, T. Dietl, G. Cywinski, C. Skierbiszewski, K. E. Spirin, V. I. Gavrilenko, S. Ruffenach, J. Torres, D. But, S. A. Dvoretsky, N. N. Mikhailov, F. Teppe, and W. Knap (unpublished).